

## Full length article

## A study of size effects in bioinspired, “nacre-like”, metal-compliant-phase (nickel-alumina) coextruded ceramics

Ryan P. Wilkerson<sup>a, b</sup>, Bernd Gludovatz<sup>c</sup>, Jeremy Watts<sup>d</sup>, Antoni P. Tomsia<sup>b</sup>, Gregory E. Hilmas<sup>d</sup>, Robert O. Ritchie<sup>a, b, \*</sup>

<sup>a</sup> Department of Materials Science & Engineering, University of California, Berkeley, CA 94720, USA

<sup>b</sup> Materials Sciences Division, Lawrence Berkeley National Laboratory, Berkeley, CA 94720, USA

<sup>c</sup> School of Mechanical and Manufacturing Engineering, UNSW, Sydney NSW 2052, Australia

<sup>d</sup> Department of Materials Science & Engineering, Missouri University of Science and Technology, Rolla, MO 65409, USA

## ARTICLE INFO

## Article history:

Received 9 November 2017

Received in revised form

4 January 2018

Accepted 5 January 2018

Available online 3 February 2018

## Keywords:

Bioinspired ceramics

Coextrusion

Strength

Toughness

## ABSTRACT

Coextrusion has been shown to be a viable processing route for the fabrication of bioinspired ceramic materials that exhibit improved damage tolerance. This provides one of the few examples of the synthesis of “nacre-like” ceramic hybrid structures with “brick-and-mortar” architectures using a method that includes the “mortar” (*i.e.*, the metallic or polymeric compliant phase) during the entire fabrication process, instead of infiltrating it into a pre-fabricated ceramic scaffold. In this study, we examine how manipulation of filament size can lead to improved mechanical performance in the resulting biomimetic ceramics by reduction of the brick size and mortar thickness while still maintaining a model high volume fraction (~90 vol.%) ceramic containing a metallic compliant phase. Specifically, we synthesized model brick-and-mortar alumina hybrid structures ( $\text{Al}_2\text{O}_3/\text{Ni}$ ) containing small volume fractions (<10%) of nickel which we made by the coextrusion of alumina and nickel oxide in a thermoplastic (polyethylene-ethyl acrylate) suspension. Flexural strength and crack-initiation fracture toughness values were used to compare the performance of various ceramic brick sizes, with full crack-growth resistance-curves (R-curves) measured and compared to similar bioinspired ceramics to ascertain how brick size and mortar thickness affect the final mechanical performance. It was found that even though these structures are significantly coarser than those made with other processing methods, they still exhibit comparable crack-growth resistance, despite their lower strength, as well as improving R-curve behavior that tracks closely with brick size. Indeed, these structures display some of the highest fracture toughness values of any high-volume fraction alumina with a metallic compliant phase to date. Toughening was found to be induced by marked crack deflection as the crack path followed the metallic “mortar” phase, coupled with significant crack bridging and “brick” pull-out in the image of the toughening mechanisms seen in nacre.

© 2018 Acta Materialia Inc. Published by Elsevier Ltd. All rights reserved.

## 1. Introduction

In many respects, ceramics represent ideal lightweight materials in terms of their high specific strengths, elastic moduli and creep resistance, coupled with low thermal expansion and good chemical resistance although, as is widely appreciated, their adoption for the vast majority of structural applications has been severely compromised by their low toughness and ductility, a product of strong bonding and a high Peierls stress, which makes

them highly flaw-sensitive. Nature, however, is remarkably adept at using brittle, ceramic-like, materials for many of its structural applications. Sea shells are a notable example in that they can display excellent strength, toughness and even wear resistance despite consisting primarily of a brittle mineral, *e.g.*, aragonite in the nacre layer of abalone shells [1–3]. The obvious success of Nature in this regard has led to an entirely new field of research endeavor, that of biomimetics, resulting in an increasing scrutiny of the structure of natural materials, such as sea shells, fish scales, bamboo, bone, teeth, and so forth, for inspiration in the design of new and improved lightweight structural (and functional) materials.

Despite a small palette of constituent materials to work with, most with meagre mechanical properties, Nature attains

\* Corresponding author. Department of Materials Science & Engineering, University of California, Berkeley, CA 94720, USA.

E-mail address: [roritchie@lbl.gov](mailto:roritchie@lbl.gov) (R.O. Ritchie).

remarkable properties and functionality by designing hybrid materials, often comprising soft and hard phases, which are assembled into a hierarchical architecture, spanning multiple length-scales, containing graded interfaces and ingenious gradients in structure, orientation and/or composition. Whereas this presents a compelling landscape for bio-inspiration, the problem in mimicking such complex hierarchies in a man-made material is in our latent inability to process them. The “top-down” fabrication/engineering approaches that are regularly used to make bulk structural materials are simply not practical for building multi-scale structural architectures with the same degree of organization as biological materials where “bottom-up” growth and adaptation are utilized. However, the development of certain materials processing technologies show promise in this regard; methods such as 3-D printing and freeze-casting are capable of making relatively large parts yet, in principle, can enable fine structural control even down to the nanoscale.

To date, significant research [4–10] has been devoted to the use of freeze-casting as a means to make bio-inspired ceramic hybrid materials, mainly in the image of the “brick-and-mortar” structure of nacre. Nacre is a highly efficient natural material in that, in energy terms, it displays a toughness which is over three orders of magnitude larger than that of its constituent phases, *i.e.*, 95 vol.% of aragonite mineral “bricks” separated by a biopolymeric “mortar”. Such damage-tolerance arises from the hard mineral bricks providing for strength, whereas *limited* sliding ( $\sim 2\ \mu\text{m}$  displacements) in the mortar allow for some ductility; the combination of these two properties generates toughness via such mechanisms as crack deflection and principally brick “pull-out” leading to crack bridging. To mimic this structure, freeze-casting (ice-templating) has frequently been used where ceramic powders, *e.g.*, alumina or silicon carbide, are suspended in water and frozen unidirectionally to create ceramic scaffolds which are the negative replica of the lamellar structure of the ice. These porous unidirectional lamellar scaffolds are subsequently pressed to form a “brick-like” structure before being finally infiltrated with a compliant phase (*i.e.*, the “mortar”). Indeed, specific results [7,8,10] using this processing method, or variants thereof, have yielded very tough ceramics, notably early studies where a freeze-cast (nacre-like) 80 vol.% alumina brick-and-mortar structure, comprising  $\sim 2\text{--}3\ \mu\text{m}$  thick bricks infiltrated with a PMMA compliant phase, was found to have exceptional fracture toughness in excess of  $30\ \text{MPa m}^{1/2}$ , although tensile strengths were relatively low ( $\sim 200\ \text{MPa}$ ).

Micromechanical modeling [11–13] though has suggested that even better properties could be obtained with a finer structure, *i.e.*, with high aspect-ratio bricks on the order of a few micrometers wide and half a micrometer thick, and with a higher volume fraction ( $>90\%$ ) of ceramic – both characteristics of natural nacre. This modeling further implies that the most significant property enhancements should be obtained using a metal, rather than polymer, mortar, as a metallic compliant phase offers greater shear and tensile resistance to excessive sliding of the bricks.

The pursuit of this ideal structure presents marked problems for the use of freeze-casting. The advantage of this technique is that it allows for the production of bulk material, as most “bottom-up” approaches, such as layer-by-layer deposition and self-assembly [14–17], are incapable of producing macroscopic samples. However, because of the necessary void space needed for complete infiltration, freeze-casting has not been successful in achieving the high ceramic volume fractions exceeding 90% required for a light-weight structural material with optimum properties; as such, freeze-cast materials are unlikely to truly mimic natural nacre. Moreover, infiltrating a metallic phase into a ceramic scaffold is inherently difficult due to poor wetting between many of the ceramic-metal combinations of interest, such as alumina and

nickel. Correspondingly, the fine-scale, brick-and-mortar structures with high ceramic content and a metallic compliant phase, which are predicted [12] to display optimal damage-tolerance, have yet to be made using freeze-casting techniques.

In our previous study, we presented an alternative bulk processing technique, coextrusion, for the synthesis of bioinspired (nacre-like) brick-and-mortar structures comprising high ( $\sim 90\ \text{vol.}\%$ ) ceramic (alumina) volume fractions with a  $\sim 10\ \text{vol.}\%$  metallic (nickel) compliant phase [18]. While not all the structures were promising, a series of microstructures with individually controlled layer alignment were shown to have increased damage tolerance and resistance-curve behavior akin to that of nacre, in a significantly coarser structure. While this structural coarseness was not ideal for mimicking nacre, the technique allowed for a high-volume fraction of ceramic with precision control of the metallic mortar content, as well as the possibility of further refinement to produce finer microstructures.

With coextrusion, ceramic core and metallic shell materials are mixed into thermoplastics to take advantage of the easy formability and malleability of the polymer [19–22]. Specifically, the use of a thermoplastic as the binder allows for relatively easy design of the ceramic or metal phases, as there is no need to find compatible dispersants or freezing parameters which are needed for freeze-casting. The method also mitigates problems of metal infiltration because it incorporates the ceramic and metallic phases from the first stages of processing, provided they can be sintered together. By suspending both materials in a thermoplastic for the green processing, it also permits easy tuning of the structure and allows for a high throughput of material. A feed rod of material is produced with a very specific core and shell diameter, while the aspect ratio is preserved through extrusion as the cross section of the rod is reduced down to a filament. It is this filament that can be sectioned into individual pieces, and therefore processed as if they were individual “bricks” in the brick-and-mortar structure. More importantly, coextrusion allows for the production of mortar coated bricks and for tight control of the volume fraction of the mortar phase, meaning low mortar volume fractions can easily be achieved through this processing method. Here we show how a successful size reduction in coextruded ceramic bricks in a bioinspired, nacre-like, alumina, with a brick-and-mortar structure containing a nickel compliant phase, can generate improved fracture toughness and strength, as compared to previously reported ceramic-metal hybrid materials.

## 2. Experimental

### 2.1. Processing

Brick-and-mortar hybrid alumina ceramics were produced through coextrusion of ceramic and thermoplastic mixtures. Initially, polyethylene-ethyl acrylate (EEA; melt index 20, Dow Chemical) binder was softened above its glass-transition temperature in a high-shear rheometer mixer (Plasti-Corder, C.W. Brabender) to a temperature of  $150\ ^\circ\text{C}$ . Alumina (A-16-SG, Almatris) with 4 vol.%  $\text{ZrO}_2$  (3YSZ, Tosoh) was incorporated into the EEA until a volume fraction of 55 vol.% solids was achieved while the rheology was controlled through minor additions of heavy mineral oil (HMO; Sigma Aldrich). This powder/binder mixture was then molded into a cylindrical core (20.4 mm) using a heated die and hydraulic ram. The process was then repeated with NiO ( $-325\ \text{mesh}$ , Alfa Aesar) to form a separate powder/binder mixture which was subsequently pressed into two half pipe shells ( $130\ ^\circ\text{C}$ , 10 tonnes,  $\sim 1\ \text{mm}$  thick) and then laminated around the core which forms the core/shell extrusion feed rod. A mortar/shell ratio of 82.5/17.5 was chosen based off of the known volume reduction of NiO to

Ni that would occur during sintering, leaving a final quantity of 10.2 vol.% of Ni within the structure. The feed rod was extruded through a heated spinneret ( $\sim 135^\circ\text{C}$ ) to form a  $500\ \mu\text{m}$  filament maintaining the same core-shell ratio (82.5/17.5) throughout the newly produced filament's cross section (Fig. 1). To aid in the orientation of filament after extrusion, the filament was tightly wound around a spool to form a ribbon which was then bonded with a spray adhesive before being sliced off as an oriented sheet of filament. From here the filament sheets were laminated to bind the parallel filaments to one another on a laminating press (model G50, Wabash MPI). The filament sheets were then cut into  $25\ \text{mm} \times 45\ \text{mm}$  sections that were either parallel, perpendicular, or  $45^\circ$  to the filament direction. These sections were laminated together with a  $45^\circ$ -layer offset to form a billet ( $120^\circ\text{C}$ , 900 kg) of oriented filaments. Billets were pyrolyzed in an air furnace ( $10^\circ\text{C}/\text{h}$  to  $600^\circ\text{C}$ , 2 h hold) to remove the EEA thermoplastic binder before sintering. The billets were then transferred to a BN-coated graphite hot-press die and placed inside a graphite hot press (Model HP20-3060, Thermal Technology Inc.) where they were heated to  $1400^\circ\text{C}$  at a rate of  $15^\circ\text{C}/\text{min}$  under flowing argon. Upon reaching temperature, a pressure of 32 MPa was applied to the die and held for 1 h after which the pressure was removed and the die was cooled to room temperature. An  $\text{Al}_2\text{NiO}_4$  spinel would form along the Ni- $\text{Al}_2\text{O}_3$  interface that was reduced during a final heat treatment in flowing Ar- $\text{H}_2$  ( $5^\circ\text{C}/\text{min}$  to  $1000^\circ\text{C}$ , 10 h hold) to reconstitute the nickel and alumina.

Two additional series were produced with the same processing

conditions. In one of these series the feed rod that was extruded through a  $300\ \mu\text{m}$  spinneret to produce  $300\ \mu\text{m}$  filament, and in the other series the feed rod was extruded through the same  $300\ \mu\text{m}$  spinneret while also being drawn onto a spool to further reduce the filament diameter down to  $200\ \mu\text{m}$ . From there the same procedure was followed with  $45^\circ$  offset layup, burnout, and final sintering. Therefore, this study was able to achieve three unique brick sizes through the control of the filament diameter of either  $500\ \mu\text{m}$ ,  $300\ \mu\text{m}$ , or  $200\ \mu\text{m}$  while still maintaining the same brick and mortar architecture.

## 2.2. Microstructural characterization

To characterize the microstructure of the three series of ceramic-metal hybrids, samples were prepared for optical and scanning electron microscopy imaging. Specimens were mechanically polished using resin bonded diamond polishing pads down to a  $1\text{-}\mu\text{m}$  diamond finish. Optical images were taken on a light microscope (Carl Zeiss Microscopy, model Lab.A1, Göttingen, Germany) for microstructural comparison. Images in the scanning electron microscope (SEM - Hitachi S-4300SE/N, Hitachi America, Pleasanton, CA, USA) were taken before and after failure in the three-point flexural tests using the secondary electron mode with a 20 keV accelerating voltage and a working distance of 12.2 mm.

Additionally, our previous study [18] showed how important mortar interconnectivity was to the brick-and-mortar behavior of the material. A similar method was followed to the previous study

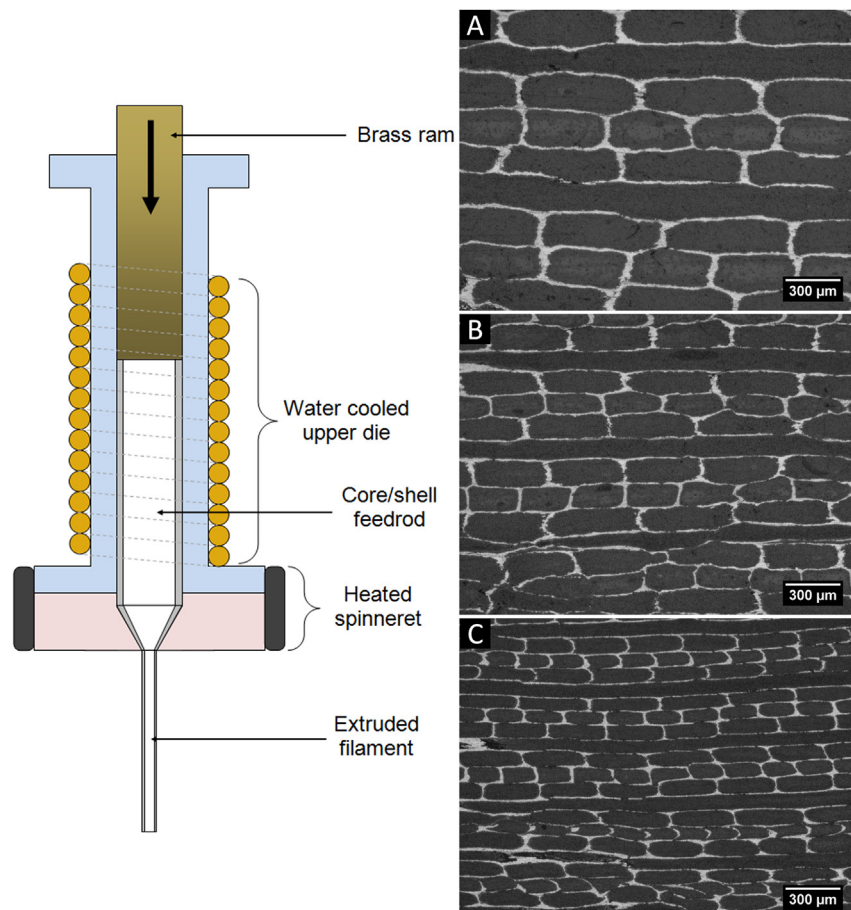


**Fig. 1.** Schematic of the coextrusion assembly, showing how the core to shell ratio is maintained from a feed rod down to a filament. Shown on the right are optical micrographs of the three  $\text{Al}_2\text{O}_3/10\text{Ni}$  metal compliant-phase ceramics made with: (A)  $500\ \mu\text{m}$  filament, (B)  $300\ \mu\text{m}$  filament, and (C)  $200\ \mu\text{m}$  filament produced through coextrusion.

using linear intercept analysis of microscope images to determine the number of brick/brick and brick/mortar interfaces and then calculation of the phase contiguity for  $\text{Al}_2\text{O}_3$  and Ni from there. These results are tabulated in Table 1 with the inclusion of the average mortar thickness as well as average brick size for comparing the structures against one another.

### 2.3. Mechanical characterization

To determine the mechanical behavior of the  $\text{Al}_2\text{O}_3/10\text{Ni}$  hybrid ceramics, beams were cut from the billets for flexural strength tests and for single edge-notched bend, SE(B), fracture toughness tests. All strength bars were cut to B-type specification (3 mm × 4 mm), in accordance with ASTM standard C1161 [23], and evaluated using a four-point flexure test. The tensile surface was aligned normal to the hot-pressing direction and polished to a 1- $\mu\text{m}$  diamond finish. Beams were loaded on an Instron 5881 electro-mechanical testing machine (Instron Corp., Norwood MA, USA) at a crosshead speed of 0.1 mm/min with upper and lower loading spans of 20 and 40 mm, respectively. Five ( $N = 5$ ) bars for each sample series were tested for average strength properties, while four ( $N = 4$ ) SE(B) bars were split between initiation toughness and R-curve analysis depending on their fracture behavior.

Fracture toughness tests on the SE(B) specimens were performed in three-point bending to determine the crack-initiation fracture toughness  $K_{Ic}$  of the hybrid ceramics, using linear-elastic fracture mechanics in accordance with ASTM standard E1820 [24]. Each beam was cut to a length of ~25 mm, with a cross-sectional width  $W = 4$  mm and thickness  $B = 4$  mm. A straight notch of 1.8 mm was cut into the tensile surface of the sample using a low speed saw with a wafering blade. The notch root was subsequently sharpened using a micro-notching technique involving polishing the root with a razor blade immersed in 3- $\mu\text{m}$  diamond solution under a constant load. This allowed for a final notch root radius below 30  $\mu\text{m}$  and a crack length,  $a$ , to width ratio,  $a/W$ , of ~0.5. The bars were polished down to a 1- $\mu\text{m}$  surface finish to minimize the effects of surface flaws during the loading of the beams. Three-point bend tests were performed with a load span of 16 mm on a screw-driven Instron 5944 testing machine.

Based on the results of these crack-initiation  $K_{Ic}$  toughness tests, full nonlinear-elastic fracture mechanics  $J$ -based crack-resistance curves,  $J_R(\Delta a)$ -curves, were determined for those samples that exhibited nonlinear load-displacement behavior in an attempt to capture both the elastic and plastic contributions to deformation and crack growth, in general accordance with ASTM standard E1820 [24]. Additional 4 mm × 4 mm bars were polished and razor notched and tested *in situ* in the Hitachi S-4300SE/N SEM using a Deben MicroTest 2 kN (Deben, UK) bending stage. This setup allows for quantitative measurement of the crack extension ( $\Delta a$ ) and the crack-growth toughness in terms of the resistance-curve (R-curve) behavior, with simultaneous real-time observation of the interaction of the crack path with the salient features of the microstructure. Samples were tested to a maximum crack extension  $\Delta a_{\text{max}}$

capacity of 550  $\mu\text{m}$ , specified by ASTM E1820 for plane-strain  $J_{Ic}$  fracture toughness measurement, where  $\Delta a_{\text{max}} = 0.25b_0$  ( $b_0$  is the initial uncracked ligament). To quote toughness in terms of the stress intensity,  $K$ , the standard mode-I  $J$ - $K$  equivalence,  $K_I = (J E')^{1/2}$ , was used to convert values of  $J_{Ic}$  to  $K_{Ic}$ , where  $E' = E$  (Young's modulus) in plane stress and  $E/(1-\nu^2)$  in plane strain ( $\nu$  is Poisson's ratio). Values of  $E$  were determined via impulse excitation and calculated with a modified long bar approximation using ASTM C1259 [25], with  $\nu$ , the Poisson's ratio for alumina, taken to be ~0.23; measured  $E$  values are listed in Table 1.

## 3. Results

### 3.1. Microstructure

As noted above, the process of coextrusion can be modified readily to change the brick morphology simply by varying the extruded filament diameter. By leaving the ceramic content and mortar-to-brick ratio constant, we produced a series of microstructures that varied only in brick size while maintaining the same architecture.

Fig. 1 shows examples of three well-formed (nacre-like) brick-and-mortar structures comprising a high-volume fraction (~90 vol.%) of alumina bricks with a metallic nickel mortar in between. The microstructural images are representative of any cut made normal to the hot-pressing direction, as the 45°-layer offset helps produce a radial symmetry akin to the platelet structure in nacre. These were made with the same ~10 vol.% nickel mortar phase using three filament diameters, specifically (A) 500  $\mu\text{m}$ , (B) 300  $\mu\text{m}$  and (C) 200  $\mu\text{m}$ , which represent the nominal brick widths. The structures were batched and processed identically, with the intent to vary only the brick size and mortar thickness. The images also indicate a well-sintered microstructure with little to no obvious porosity.

While the structures varied in brick size and mortar thickness, it is important to note that mortar interconnectivity and brick aspect ratio were not affected detrimentally during the processing. Microstructural data, listed in Table 1, indicate the aspect ratios of the  $\text{Al}_2\text{O}_3$  bricks, their size and the mortar thickness. While the average brick size is reduced by 35% between 500 and 300  $\mu\text{m}$  series, and 41% between the 300 and 200  $\mu\text{m}$  series, the aspect ratios vary only slightly (2.35–2.51). The mortar thickness follows a similar downward trend from 17.9  $\mu\text{m}$  to 11.7  $\mu\text{m}$  to 6.9  $\mu\text{m}$ , which is expected with the reduced filament thickness. Additionally, in our previous study [18] it was noted that a high contiguity, and therefore a high matrix interconnectivity, of the matrix phase trended positively with the overall mechanical behavior of the resulting hybrid structure. The measured contiguity of the three structures also shows little to no variation (0.886–0.938) which was well within the acceptable range seen in the previous study. Hence, these structures were expected to less likely result in the fracture of bricks, but rather to induce crack deflection along the brick/mortar interfaces or preferably within the mortar itself.

**Table 1**  
Microstructural information for the three Ni compliant-phase ceramic structures, shown in Fig. 1A–B and developed by coextrusion of different filament diameters.

Structure	Ni Contiguity ( $C_{\text{Ni}}$ )	Continuous Volume Ni ( $f_{\text{NiC}}$ ) <sup>a</sup>	Mortar Thickness ( $\mu\text{m}$ )	Brick Thickness ( $\mu\text{m}$ )	Brick Width ( $\mu\text{m}$ )	Width/Thickness	Elastic Modulus (GPa)
200 $\mu\text{m}$	0.886	9.03%	6.9 ± 1.4	74.2 ± 7.0	186.4 ± 12.8	2.51	318
300 $\mu\text{m}$	0.894	9.11%	11.7 ± 3.9	125.3 ± 15.0	292.9 ± 23.0	2.34	215
500 $\mu\text{m}$	0.938	9.56%	17.9 ± 3.8	182.2 ± 15.6	430.7 ± 18.1	2.36	227

<sup>a</sup> Possible maximum is 10.2%.

### 3.2. Mechanical characterization – strength and toughness

Four-point bend tests were performed to determine the flexural strength of the three unique microstructures; results are shown by the blue columns in the histogram in Fig. 2. As the brick size decreases we see strength trend upwards from  $110 \pm 8$  MPa for the 500  $\mu\text{m}$  structure up to  $158 \pm 24$  MPa for the 200  $\mu\text{m}$  structure with the 300  $\mu\text{m}$  structure in between the two at  $113 \pm 18$  MPa. Although these flexural strengths show a ~45% increase with a 60% decrease in brick size, these values are lower than the strength of pure alumina (~400 MPa), results which are not unexpected as similar numbers were found in our prior study [18] of coextruded alumina/Ni hybrid ceramics.

Corresponding evaluation of the toughness of these ceramic-Ni hybrids was made initially on linear-elastic fracture mechanics tests in micro-notched three-point bending to measure  $K_{Ic}$  values; such crack-initiation values are shown by the pink columns in the histogram in Fig. 2. Akin to the flexural strengths, the toughness of the brick-and-mortar structures strongly correlates with reduced brick size. Specifically,  $K_{Ic}$  values increase just over 20%, from  $3.4 \text{ MPa m}^{1/2}$  to  $4.1 \text{ MPa m}^{1/2}$ , with a 60% reduction in brick size from nominally 500  $\mu\text{m}$  to 200  $\mu\text{m}$ , respectively.

However, as the principal contributions to toughness in such brick-and-mortar ceramics are achieved extrinsically<sup>1</sup> during crack growth, additional nonlinear-elastic  $J_R$ -curve measurements were performed to measure resistance-curve behavior as a basis of evaluating the crack-growth toughness of these structures. Resulting R-curves, generated by *in situ* testing in three-point bending in the SEM with real time observations of crack growth, are shown in Fig. 3, and are expressed in terms of stress-intensity  $K_I$  values. As was mentioned earlier, the maximum valid  $K_I$  value that can be obtained from R-curve analysis is given at  $\Delta a_{\text{max}} = 0.25b_0$ , which is ~550  $\mu\text{m}$  in the case of these specimens. All three structures showed marked rising R-curve behavior with the crack-growth toughness being inversely related to the fineness of the microstructures. Defined in terms of the slope of the R-curves, strictly “valid” crack-growth toughness values varied from  $6.6 \text{ MPa m}^{1/2}$  in the 500- $\mu\text{m}$  brick sized structures to  $12.6 \text{ MPa m}^{1/2}$  in the 200  $\mu\text{m}$  structures, a 92.6% increase in toughness for a 60% decrease in brick size. Although monolithic alumina tends to fracture catastrophically, all three nacre-like structures were able to sustain stable crack extensions in excess of  $\Delta a \sim 1 \text{ mm}$ , with toughness values well in excess of  $15 \text{ MPa m}^{1/2}$ , i.e., at least a factor of two greater than any reported toughness values for monolithic alumina (Fig. 3).

### 3.3. Crack-growth observations

Corresponding observations of the crack paths during the *in situ* measurements of R-curves in the SEM are shown in Fig. 4. While cracks were observed to pass through the bricks on occasion, the majority of the crack advance was primarily to follow the mortar phase; this can lead to significant crack deflection away from the plane of maximum stress, particularly for the 200 and 300  $\mu\text{m}$

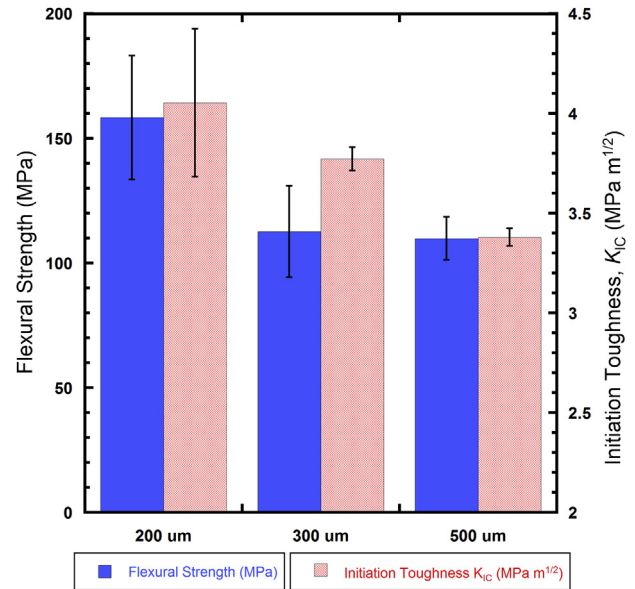


Fig. 2. Four-point flexural strength for the three microstructures shows a ~45% increase with a 60% decrease in brick size from 500 to 200  $\mu\text{m}$ . Corresponding crack-initiation  $K_{Ic}$  fracture toughness values increase by just over 20% for the same decrease in brick size, indicating an improved overall mechanical performance as the brick-and-mortar structure is refined.

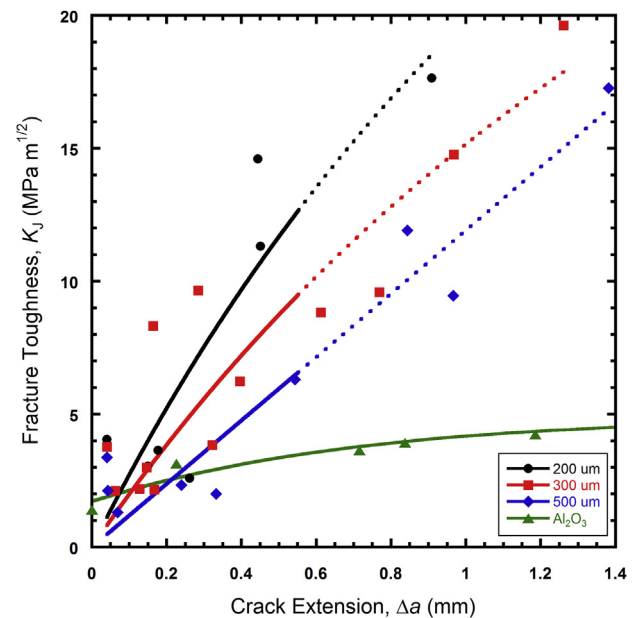
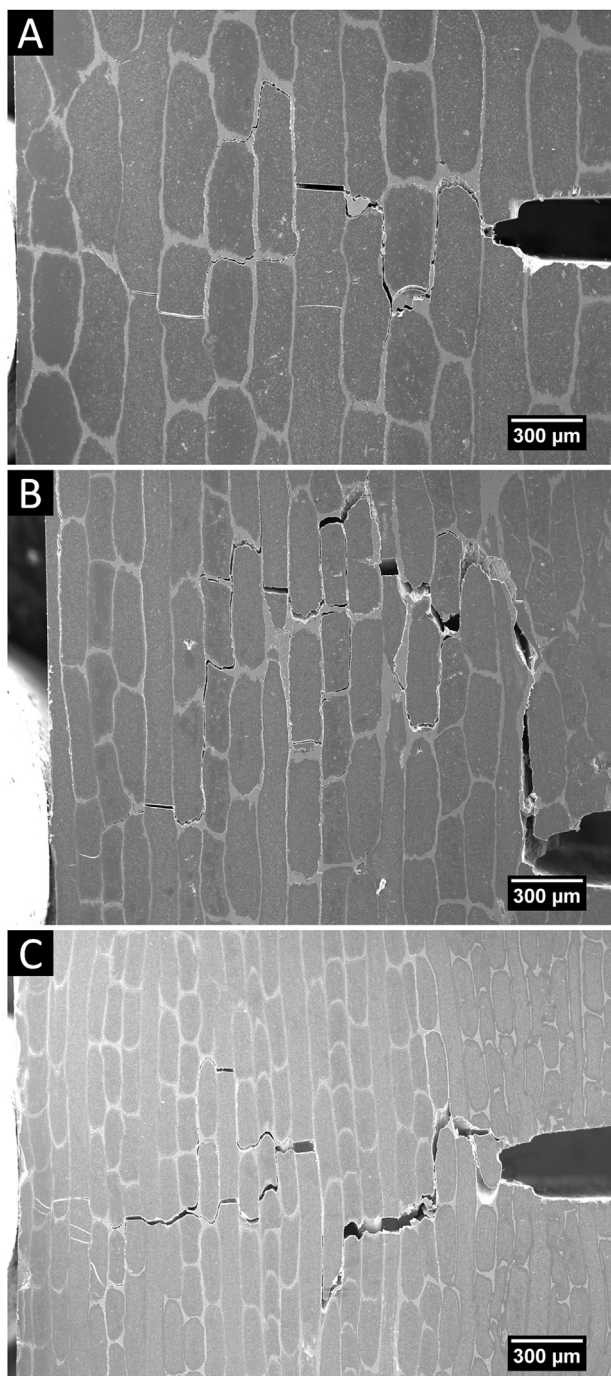


Fig. 3. Crack-growth resistance (R-) curves measured using *in situ* three-point bend tests in the SEM. Results were obtained using nonlinear elastic fracture mechanics in terms of  $J$ , which were then converted into stress intensity  $K_I$  values (see text). All three structures, with brick sizes varying between 200 and 500  $\mu\text{m}$ , can be seen to exhibit rising R-curve behavior with  $K_I$  values exceeding  $15 \text{ MPa m}^{1/2}$ ; there is further a clear trend of steeper curves with decreasing brick size. Compared against these three structures is that of pure  $\text{Al}_2\text{O}_3$  [27] which has a very shallow, almost flat R-curve.

<sup>1</sup> Resistance to fracture can be considered as a mutual competition between two classes of toughening mechanisms: *intrinsic* mechanisms, which represent material's inherent resistance to microstructural damage mechanisms that operate ahead of the crack tip, plasticity (or some form of inelasticity) being the dominant contributor, and *extrinsic* mechanisms, which act to “shield” the crack from the applied driving force and operate principally in the wake of the crack tip. Extrinsic toughening mechanisms, such as crack deflection and crack bridging, are the prime toughening mechanisms in most brittle materials. They are only effective in developing crack-growth toughness, as demonstrated by a rising R-curve, and have little to no influence on the crack-initiation toughness [26].

brick-sized microstructures. The existence of mortar layers perpendicular to the growing crack were also seen to cause crack bifurcation, leading to increased microcracking (Fig. 4). This enhanced tortuosity in crack paths, especially in the finer microstructures, results in the phenomenon of brick pull-out – this is particularly noticeable for the 200  $\mu\text{m}$  brick size – which results in



**Fig. 4.** Scanning electron micrographs of one of the 500  $\mu\text{m}$  (A), 300  $\mu\text{m}$  (B), and 200  $\mu\text{m}$  (C) specimens after *in situ* fracture analysis. In the 500  $\mu\text{m}$  specimen, crack deflection can be seen above and below the crack root, with minimal cracking through the bricks. While the 300  $\mu\text{m}$  specimen shows significantly more crack deflection above the crack root with noticeable crack bifurcation and crack bridging in this region. Finally, in the 200  $\mu\text{m}$  sample the crack deviates somewhat from the plane of maximum tensile stress as there is extensive mortar delamination and crack deflection as well as multiple bricks bridging the crack path.

significant crack bridging. As in nacre [28], this is likely to be the primary toughening mechanism in these structures. Specifically, the finer the structure the more tortuous the observed crack paths, with the 200  $\mu\text{m}$  series having extensive crack deflection and brick pullout. Indeed, both of these extrinsic toughening mechanisms, *i.e.*, crack deflection and brick pull-out/crack bridging, are

characteristic of natural nacre, and contribute to the steeply rising R-curve behavior of these nacre-like ceramic-Ni hybrids.

Crack deflection is also quite significant in these structures, although this invariably occurs via interfacial delamination, as can be seen in Fig. 5 where there is little to no evidence of ductile failure in the mortar. Limited “inter-brick” displacements are essential to create ductility (and hence toughness); however, to utilize the increased shear/tensile resistance of the metallic mortar for optimum toughness, such displacements would be better achieved within the mortar, rather than along mortar/brick interfaces.

To gain some bearing as to how weak these mortar/brick interfaces in these structures are, the He and Hutchison [29] analysis was used. This defines the (elastic) conditions for an impinging crack to either penetrate through a dissimilar material interface or arrest/delaminate along the interface, and as such can be used to estimate the interfacial toughness [30] (Fig. 6). Two factors determine whether or not the crack will delaminate along the interface: (i) the elastic mismatch of the two materials, given by the first Dundurs' parameter,  $\alpha = (E_1 - E_2)/(E_1 + E_2)$ , where  $E_1$  and  $E_2$  are the Young's moduli of the two materials [31], and (ii) the ratio of the interfacial toughness to the toughness of material 2 which the crack would enter if it penetrated the interface,  $G_{c,\text{interf}}/G_{c2}$ , where toughness values are expressed in terms of the strain energy release rate  $G$ . For a crack originating in the alumina traveling into the nickel mortar,  $\alpha \sim -0.26$ , the estimation of an upper-bound for the toughness of the interface is given by  $G_{c,\text{interf}}/G_{c2} \sim 0.23$ . This was confirmed by creating a Vickers indent at a load of over 10 N in the alumina to generate cracks which are directed to impinge roughly normally on the nickel/alumina interface (Fig. 6); these cracks can be seen to not penetrate the interface but rather to become arrested and form interface delamination cracks. Using a value of 0.031  $\text{kJ}/\text{m}^2$  for the toughness of the alumina, Table 2 lists the data measured using this approach, which gives an upper-bound estimate of the interfacial toughness of 21.8  $\text{kJ}/\text{m}^2$ .

#### 4. Discussion

Coextrusion is a unique processing method that can be used to make, and subsequently tune, the architecture of nacre-like, brick-and-mortar ceramic-metal hybrid structures through the production of a mortar-coated ceramic filament. Methods such as chopping the filament into individual bricks as well as compressing them individually to further increase the aspect ratio have been

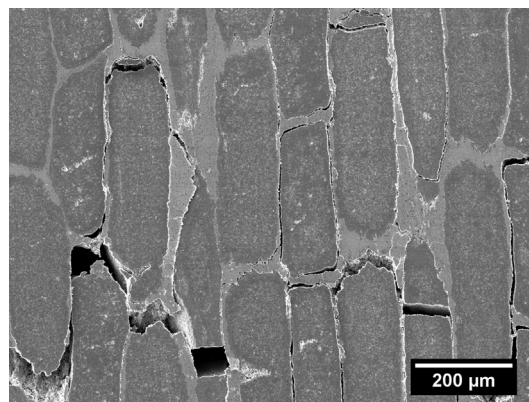


**Fig. 5.** SEM micrograph of a 300  $\mu\text{m}$  specimen showing the extent of interfacial delamination in the crack wake. While the inclusion of a metallic mortar was intended as a means of introducing a ductile failure mechanism into the structure, when weak interfaces are present there is little evidence of plasticity in the failure region and the crack travels along the interface instead. This behavior is inherent in all three structures produced by this method.

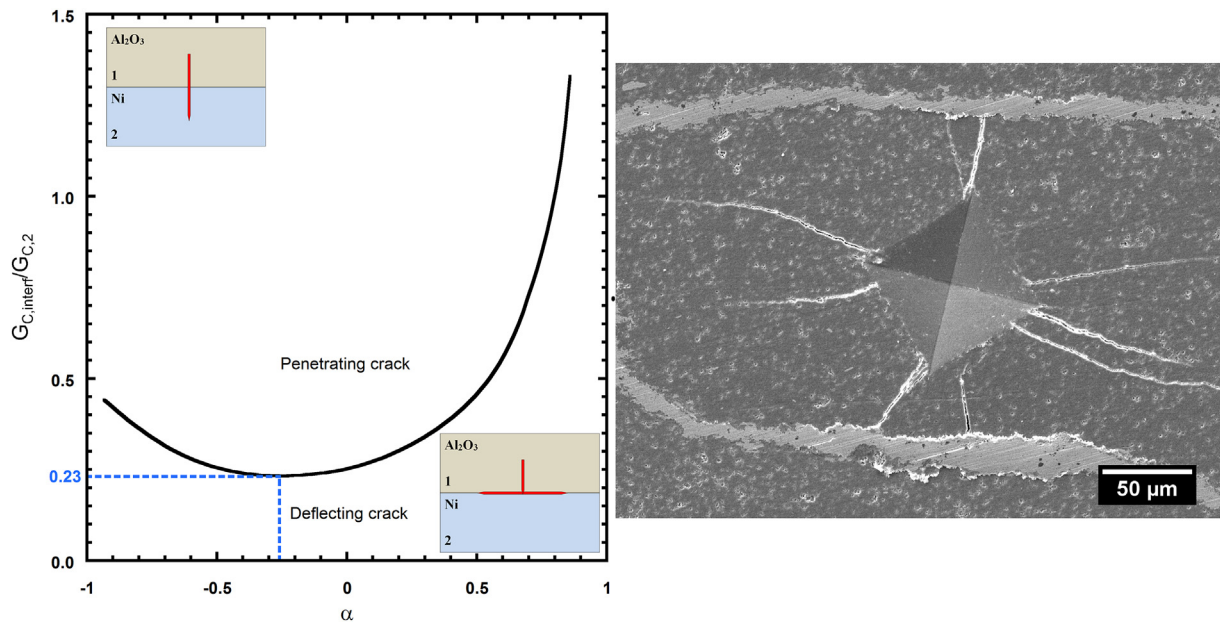


**Fig. 6.** A plot of the linear elastic solutions of He and Hutchinson [29] which show the conditions where a crack impinging normally on a dissimilar material interface between materials 1 and 2 will either penetrate the interface or arrest/deflect along the interface. For a  $-90^\circ$  incident crack angle, two factors determine whether or not the crack will penetrate: (i) the elastic mismatch between the two materials which is given by the first Dundurs' parameter  $\alpha = (E_1 - E_2)/(E_1 + E_2)$ , where  $E_1$  and  $E_2$  are the Young's moduli of the two materials [31], and (ii) the ratio of the interfacial toughness to the toughness of material 2 which the crack would enter if it penetrated the interface,  $G_{C,interf}/G_{C,2}$ . For a penetrating crack originating in the alumina traveling into the nickel mortar,  $\alpha \sim -0.26$ . If cracks emanating from Vickers hardness indents in the alumina are directed to impinge normally on the nickel/alumina interface, as the right-hand micrograph shows, they do not penetrate the interface but rather form delamination cracks along the interface. This allows for the estimation of an upper-bound toughness of the nickel/alumina interface of  $G_{C,interf} \sim 0.23$ .

**Table 2**

Tabulated data for the interfacial toughness, determined using the He-Hutchinson analysis [29].

	Toughness, $G_C$ (kJ/m <sup>2</sup> ) <sup>a</sup>	Toughness, $K_{Ic}$ (MPa.m <sup>1/2</sup> )
Al <sub>2</sub> O <sub>3</sub>	0.031	3.49
Nickel	94.2	146.9
Al <sub>2</sub> O <sub>3</sub> /Ni Interface	<21.8	–

<sup>a</sup>  $K_{Ic}$  values for alumina were measured directly in this study, whereas a value for the toughness of nickel was taken from Ref. [32]. These values were then converted to strain energy release rates ( $G_C$ ). It should be noted that the interfacial toughness can only be determined as an upper-bound.

explored in detail previously [18]. However, it was found that simply laying up the filament layer by layer at variable offset angles was particularly effective at producing brick-and-mortar architectures, but also in developing desired mechanical properties, in particular crack-growth resistance in terms of inhibiting catastrophic fracture from unstable growth of incipient cracks. This was related to a combination of two factors: a high degree of mortar interconnectivity and the increase in the brick aspect ratio via the brick length. Adjusting the filament diameter was the next logical progression for the development of these brick-and-mortar architectures. Varying the filament diameter provided a means to reduce the overall brick size without the detrimental effects of limited mortar interconnectivity that were seen previously using additional manipulation of the filament post extrusion [18]. Accordingly, three microstructures were produced by the filament layup method with excellent looking brick-and-mortar structures, with brick sizes varying between 500 and 200  $\mu\text{m}$  (Fig. 1).

The structure of these coextruded alumina-Ni hybrids, while mimicking the relative proportion of bricks to mortar in nacre, are obviously definitely far coarser than the natural material. In terms of properties, this is reflected in their low flexural strengths which, as in our previous study [18], remain under 200 MPa. This is clearly

a drawback with coextrusion processing although the current results unambiguously indicate that both strength and toughness properties are improved by refining the brick size. The advantage of coextrusion though is that it enables the processing of seemingly perfect, albeit coarse, model brick-and-mortar structures in the true image of nacre with a high-volume fraction of ceramic exceeding 90% together with a metallic mortar. Based on micro-mechanical modeling [12], this should represent the ideal structure, and indeed these alumina-Ni hybrids do display excellent toughness with R-curve fracture toughness values exceeding 15 MPa m<sup>1/2</sup>; this is the highest fracture toughness reported to date for a high-volume fraction alumina with a metallic compliant phase. This is achieved by the relative absence of brick fracture, and the occurrence of shear displacements in the mortar regions, leading to crack deflection, crack-path tortuosity, brick pull-out and consequent crack bridging. As in nacre [28], such bridging is likely to be the primary toughening mechanism, resulting in the steep rising R-curve behavior in these structures (Fig. 3). This stabilizes the subcritical extension of cracks, thereby avoiding unstable catastrophic failure of the ceramic. However, one must still question why these toughness values, although high, still do not approach the levels attained using brick-and-mortar alumina structures containing a polymeric (PMMA) mortar where measured toughness values were significantly larger [4].

The reason for this appears to be that although both the polymer and metallic mortars provide for inter-brick displacement to minimize brick fracture, which initiates the brick pull-out that is the origin of toughening by crack bridging, these displacements occur *within* the mortar when polymers are used as the compliant phase, whereas in the present case with a Ni mortar, the majority of the inter-brick displacement takes place along the Ni-alumina interface rather than within the metallic phase. It should be noted that polymer/PMMA interfaces were intentionally made strong, using techniques such as grafting [9,33], to force the inter-

brick displacements to occur within the mortar, where the toughening can be augmented by the creation of damage in the layer and additionally by the resistance of the mortar itself to shear (and also tension for the vertical mortar regions). The potentially enhanced toughening effect of a metallic mortar is in its greater strength, in terms of higher resistance to tension and shear, as compared to a polymer like PMMA, although the mortar strength cannot, of course, exceed the strength of the ceramic or else brick fracture would ensue, which would completely compromise the strength and toughness of the material. Inter-brick displacements along the ceramic/mortar interfaces, as with the present materials, still protect the bricks from fracture and as such create the conditions for toughening by crack deflection and bridging, but such cracking along the interfaces serves to curtail the additional toughening from the shear/tensile resistance of the mortar. Indeed, this is also the prime reason for the lower strength of our materials.

To determine why the nickel/alumina interface was much weaker than the nickel, further examination was performed to measure the maximum interfacial toughness; a value of  $\sim 21.8 \text{ kJ/m}^2$  was obtained which is, at best, less than 25% of the toughness of nickel. Further investigation using SEM analysis yielded interesting results when comparing secondary to backscatter images where backscatter can produce higher elemental contrast. Fig. 7 shows a noticeable difference between the secondary (A) and backscatter (B) images, specifically the presence of an intermediate region between the nickel and alumina. High-resolution images of this region (D) show that it consists of alumina grains with interdispersed nickel along the grain boundaries, likely a remnant of the decomposition reaction of  $\text{Al}_2\text{NiO}_4$  spinel during processing. Cracks travel primarily along the interface between the nickel and the reaction region (C), but it is not clear if the presence of this reaction region is the cause of the weak interface, as highly tortuous interfacial regions between nickel and alumina have been attributed in the past to reduced mechanical performance [34].

What we learn from this is that to create lightweight structural materials with  $>90 \text{ vol.}\%$  ceramic materials using bioinspired

(nacre-like) brick-and-mortar structures, the use of metallic mortars offers the greatest potential, both in terms of its higher temperature capability and that theoretically it should attain higher strength and toughness; however, to realize such high toughness without diminishing strength, it will be necessary to not only refine the brick widths to less than  $10 \mu\text{m}$  or so, which incidentally would be difficult using the coextrusion methodology, but also to develop such ceramic/compliant metal phase structures where the ceramic/metal interface is strong enough for the inter-brick displacements to be confined within the metal mortar, yet not too strong to cause brick failure. To date, no one has achieved this ideal bioinspired structure.

## 5. Conclusions

In this study, using coextrusion we have developed and processed a nacre-like brick-and-mortar architecture of an alumina (brick-like) microstructure containing a metallic nickel compliant (mortar) phase, where we have been able to refine the ceramic brick size by varying the coextruded filament diameter. While coextrusion produces structures that are significantly coarser than naturally-occurring nacre, these drawbacks are somewhat mitigated by the high degree of tunability that can be achieved. The method enabled the production of  $>90 \text{ vol.}\%$  ceramic brick-and-mortar microstructures, containing a  $<10 \text{ vol.}\%$  metallic mortar and bricks ranging in size from  $\sim 180$  to  $430 \mu\text{m}$ , that exhibit marked crack-growth resistance with toughness values exceeding  $15 \text{ MPa m}^{1/2}$  (compared to values of  $\sim 5 \text{ MPa m}^{1/2}$  for monolithic alumina). The resulting nacre-like alumina-nickel structures processed in this study all exhibited:

- significant resistance to crack growth and failure, *i.e.*, steeply rising R-curve behavior,
- strength, crack-initiation  $K_{Ic}$  toughness and crack-growth toughness on the R-curve that increased with decreasing brick size,

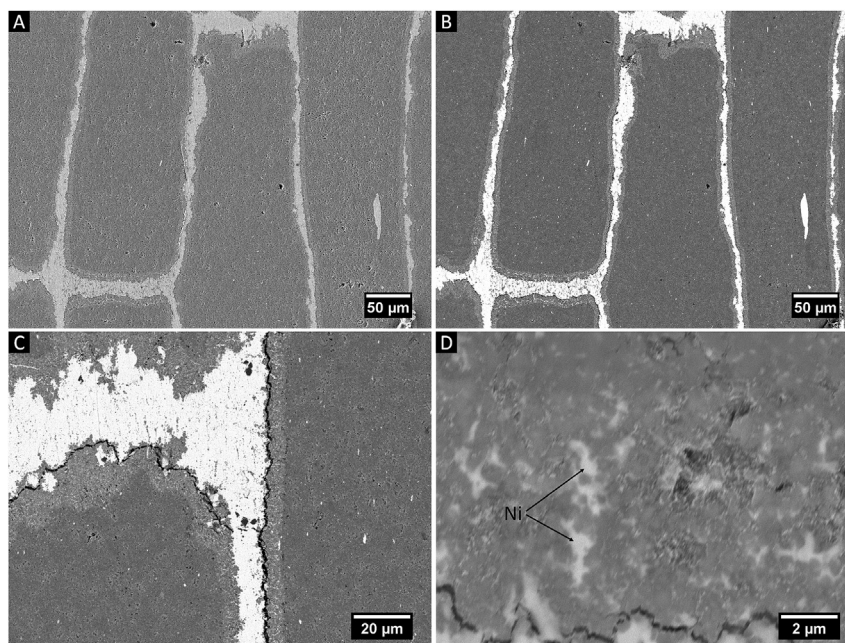


**Fig. 7.** Comparison SEM micrographs imaged using secondary electron (SE) imaging (A) and backscatter electron (BSE) imaging (B) showing the presence of a region between the alumina bricks and nickel mortar. Backscatter images (C) show that the cracks traverse along the interface between the reaction region and the nickel mortar; higher-resolution imaging (D) indicates that the region is comprised of alumina grains with the nickel in the grain boundaries providing the higher elemental contrast with BSE. This is likely a remnant of the decomposition reaction that occurs during the final heat treatment to reduce the nickel aluminate spinel formed during sintering back into nickel and alumina.

- R-curve toughness exceeding 15 MPa m<sup>1/2</sup>.

Although the present model alumina/Ni-metal brick-and-mortar structures are clearly coarse, they nevertheless displayed excellent toughness compared to monolithic alumina, but with low flexural strength. However, we believe that these structures have the potential with metallic mortars to achieve significantly higher toughness and strength. This is because in the present materials, the limited inter-brick displacements, which are absolutely vital to attain the required toughness by stabilizing subcritical cracking without catastrophic fracture, largely occurred along the ceramic-metal interfaces. To utilize the full potential of the shear/tensile strength of metallic mortars, these inter-brick displacements need to be within the mortar, which can only be effectively achieved by finding a means of strengthening these biomaterial interfaces. This will both significantly elevate the strength and potentially further enhance the already high toughness of these compliant-phase ceramics.

### Acknowledgements

This work was supported by the Mechanical Behavior of Materials Program (KC-13) at the Lawrence Berkeley National Laboratory, funded by the U.S. Department of Energy, Office of Science, Office of Basic Energy Sciences, Materials Sciences and Engineering Division, under contract no. DE-AC02-05CH11231. The authors would also like to thank their collaborators at Missouri University of Science and Technology in Rolla, MO for the use of their facilities.

### References

- [1] U.G.K. Wegst, H. Bao, E. Saiz, A.P. Tomsia, R.O. Ritchie, Bioinspired structural materials, *Nat. Mater.* 14 (2015) 23–36.
- [2] U.G.K. Wegst, M.F. Ashby, The mechanical efficiency of natural materials, *Philos. Mag* 84 (2004) 2167–2181.
- [3] C. Wang, Y. Huang, Q. Zan, H. Guo, S. Cai, Biomimetic structure design—a possible approach to change the brittleness of ceramics in nature, *Mater. Sci. Eng. C* 11 (2009) 9–12.
- [4] E. Munch, M.E. Launey, D.H. Alsem, E. Saiz, A.P. Tomsia, R.O. Ritchie, Tough bio-inspired hybrid materials, *Science* 322 (2008) 1516–1520.
- [5] O.O. Ekiz, A.F. Dericioglu, H. Kakisawa, An efficient hybrid conventional method to fabricate nacre-like bulk nano-laminar composites, *Mater. Sci. Eng. C* 29 (2009) 2050–2054.
- [6] M.E. Launey, E. Munch, D.H. Alsem, E. Saiz, A.P. Tomsia, R.O. Ritchie, A novel biomimetic approach to the design of high-performance ceramic–metal composites, *J. Roy. Soc. Interface* 7 (2010) 741–753.
- [7] F. Bouville, E. Maire, S. Meille, B. Van de Moortèle, A.J. Stevenson, S. Deville, Strong, tough and stiff bioinspired ceramics from brittle constituents, *Nat. Mater.* 13 (2014) 508–514.
- [8] V. Naglieri, B. Gludovatz, A.P. Tomsia, R.O. Ritchie, Developing strength and toughness in bio-inspired silicon carbide hybrid materials containing a compliant phase, *Acta Mater.* 98 (2015) 141–151.
- [9] H. Bai, F. Walsh, B. Gludovatz, B. Delattre, C. Huang, Y. Chen, A.P. Tomsia, R.O. Ritchie, Bioinspired hydroxyapatite/poly(methyl methacrylate) composite with a nacre-mimetic architecture by a bidirectional freezing method, *Adv. Mater.* 28 (2016) 50–56.
- [10] H. Zhao, Y. Yue, L. Guo, J. Wu, Y. Zhang, X. Li, S. Mao, X. Han, Cloning nacre's 3D interlocking skeleton in engineering composites to achieve exceptional mechanical properties, *Adv. Mater.* 28 (2016) 5099–5105.
- [11] F. Barthelat, H. Tang, P.D. Zavattieri, C.M. Li, H.D. Espinosa, On the mechanics of mother-of-pearl: a key feature in the material hierarchical structure, *J. Mech. Phys. Solid.* 55 (2007) 306–337.
- [12] M.R. Begley, N.R. Phillips, B.G. Compton, D.V. Wilbrink, R.O. Ritchie, M. Utz, Micromechanical models to guide the development of synthetic 'brick and mortar' composites, *J. Mech. Phys. Solid.* 60 (2012) 1545–1560.
- [13] N. Sakhavand, R. Shahsavari, Universal composition–structure–property maps for natural and biomimetic platelet–matrix composites and stacked heterostructures, *Nat. Comm* 6 (2015), 6523.
- [14] L.J. Bonderer, A.R. Studart, L.J. Gauckler, Bioinspired design and assembly of platelet reinforced polymer films, *Science* 319 (2008) 1069–1073.
- [15] W. Cui, M. Li, J. Liu, B. Wang, C. Zhang, L. Jiang, Q. Cheng, A strong integrated strength and toughness artificial nacre based on popamine cross-linked graphene oxide, *ACS Nano* 8 (2014) 9511–9517.
- [16] H. Zhao, Y. Yue, Y. Zhang, L. Li, L. Guo, Ternary artificial nacre reinforced by ultrathin amorphous alumina with exceptional mechanical properties, *Adv. Mater.* 28 (2016) 2037–2042.
- [17] K. Chen, X. Tang, Y. Yue, H. Zhao, L. Guo, Strong and tough layered nanocomposites with buried interfaces, *ACS Nano* 10 (2016) 4816–4827.
- [18] R.P. Wilkerson, B. Gludovatz, J. Watts, A.P. Tomsia, G.E. Hilmas, R.O. Ritchie, A novel approach to developing biomimetic ("nacre-like") metal-compliant-phase (nickel–alumina) ceramics through coextrusion, *Adv. Mater.* 28 (2016) 10061–10067.
- [19] J.W. Zimmermann, G.E. Hilmas, W.G. Fahrenholtz, Thermal shock resistance and fracture behavior of ZrB<sub>2</sub>-based fibrous monolith ceramics, *J. Am. Ceram. Soc.* 92 (2009) 161–166.
- [20] J. Watts, G.E. Hilmas, Processing and indentation behavior of functionally designed cellular cemented carbides produced by coextrusion, *Int. J. Refract. Met. H* 24 (2006) 229–235.
- [21] S. Baskaran, S.D. Nunn, J.W. Halloran, Fibrous monolithic ceramics: IV, Mechanical properties and oxidation behavior of the alumina/nickel system, *J. Am. Ceram. Soc.* 77 (1994) 1256–1262.
- [22] G. Hilmas, A. Brady, U. Abdali, G. Zywichi, J. Halloran, Fibrous monoliths: non-brittle fracture from powder-processed ceramics, *Mater. Sci. Eng. A* 195 (1995) 263–268.
- [23] ASTM Standard C1161, Flexural Strength of Advanced Ceramics at Ambient Temperature, vol. 2003, ASTM International, West Conshohocken, PA, 2013, <https://doi.org/10.1520/C1161-13>. [www.astm.org](http://www.astm.org).
- [24] ASTM Standard E1820, Measurement of Fracture Toughness, vol. 2003, ASTM International, West Conshohocken, PA, 2016, <https://doi.org/10.1520/E1820-16>. [www.astm.org](http://www.astm.org).
- [25] ASTM Standard C1259, Dynamic Young's Modulus, Shear Modulus, and Poisson's Ratio for Advanced Ceramics by Impulse Excitation of Vibration, vol. 2003, ASTM International, West Conshohocken, PA, 2015, <https://doi.org/10.1520/C1259-15>. [www.astm.org](http://www.astm.org).
- [26] R.O. Ritchie, The conflict between stress and toughness, *Nat. Mater.* 10 (2011) 817–822.
- [27] J.J. Kruzic, R.M. Cannon, R.O. Ritchie, Effects of moisture on grain-boundary strength, fracture, and fatigue properties of alumina, *J. Am. Ceram. Soc.* 88 (2005) 2236–2245.
- [28] Y. Shao, H.P. Zhao, X.Q. Feng, H. Gao, Discontinuous crack-bridging model for fracture toughness analysis of nacre, *J. Mech. Phys. Solid.* 60 (2012) 1400–1419.
- [29] M.Y. He, J.W. Hutchinson, Crack deflection at an interface between dissimilar elastic materials, *Int. J. Solid Struct.* 25 (1989) 1053–1067.
- [30] V. Imbeni, J.J. Kruzic, G.W. Marshall, S.J. Marshall, R.O. Ritchie, The dentin-enamel junction and the fracture of human teeth, *Nat. Mater.* 4 (2005) 229–232.
- [31] J. Dundurs, Discussion: edge-bonding dissimilar orthogonal elastic wedges under normal and shear loading, *J. Appl. Mech.* 36 (1969) 650–652.
- [32] A. Hohenwarter, R. Pippin, Fracture toughness evaluation of ultrafine-grained nickel, *Scripta Mater.* 64 (2011) 982–985.
- [33] M.E. Launey, R.O. Ritchie, On the fracture toughness of advanced materials, *Adv. Mater.* 21 (2009) 2103–2110.
- [34] Z. Chen, J.J. Mecholsky, Control of strength and toughness of ceramic/metal laminates using interface design, *J. Mater. Res.* 8 (1993) 2362–2369.